Chemical Engineering Journal 451 (2023) 138663

Contents lists available at ScienceDirect

Chemical Engineering Journal

journal homepage: www.elsevier.com/locate/cej

Interface regulation of Mg anode and redox couple conversion in cathode by copper for high-performance Mg-S battery

Rupeng Zhang, Can Cui, Rang Xiao, Ruinan Li, Tiansheng Mu *, Hua Huo, Yulin Ma, Geping Yin, Pengjian Zuo *

MIIT Key Laboratory of Critical Materials Technology for New Energy Conversion and Storage, School of Chemistry and Chemical Engineering, Harbin Institute of Technology, Harbin 150001, PR China

ARTICLE INFO

Keywords:
Mg-S battery
Artificial interphase
$Mg(TFSI)_2$-based electrolytes
Copper powders

ABSTRACT

The Mg-S battery has great development potential benefiting from its high volume energy density and high-safety. However, it also confronts with two key issues especially when using the $Mg(TFSI)_2$-based electrolyte. One is the poor compatibility between electrolyte and Mg anode, and the other is the poor reversibility of cathode. In this work, an artificial interphase including $Zn/ZnCl_2/MgZn_2/MgCl_2$ was firstly pre-constructed by replacement reaction of $ZnCl_2$ and Mg, which can reduce Mg plating/stripping overpotential to 0.2 V at 0.1 mA/cm^2. Meanwhile, the reversibility of cathode can be improved by using copper powders as additive in sulfur/carbon composite cathode, and the improvement effect is directly related to the addition amount and particle size of copper powders. In addition, it is also revealed that the chemical reaction can occur between copper and intermediates MgS_8 at the initial stage of discharge process. The reaction product of Cu_2S continues to participate in the electrochemical reduction reaction to regenerate copper, which can be reoxidized to Cu_2S during the charging process. The conversion of redox couple from S/S^{2-} to Cu_2S/Cu^0 in cathode improves the cycling stability of the battery in comparison with the conversional Mg-S battery.

1. Introduction

Rechargeable Mg metal batteries (RMMBs) have great development potential and application value benefiting from several unique properties. Specifically, Mg metal is endowed with the characteristics of high theoretical specific capacity (2205 mAh g^{-1} and 3833 mAh cm^{-3}), low reduction potential (-2.36 V vs SHE), and abundant resource (2.3 wt% in the earth's crust), which make it suitable as anode for low-cost and high energy density electrochemical devices [1]. More importantly, in terms of safety concerns, Mg metal electrode shows exceptional advantage over other alkaline metal electrodes (Li, Na or K, etc.) by reason that the low dendrite formation tendency will help eliminate the potential safety hazards [2]. Meanwhile, the choice of cathode materials is also crucial to the energy density of RMMBs[3,4]. Among all the cathode materials proposed at present, the sulfur cathode undoubtedly has great potential by virtue of its high theoretical specific capacity (1675 mAh g^{-1}) based on two-electron conversation reaction of S^{2-}/S^0[5–7]. Theoretically, when coupling of Mg metal anode and sulfur cathode, the several significant characteristics of high energy density (1722 Wh kg^{-1} or 3221 Wh L^{-1}), high safety and low cost can be endowed to Mg-S battery [8,9], which is regarded as one of the most promising next-generation energy storage systems.

In fact, the development of Mg-S battery is still in its infancy, and there are still some key issues urgently to be resolved, such as the lack of suitable electrolytes [10]. To be specific, the Grignard reagent and Grignard-like reagent dissolved in aprotic solvents such as APC-type ("All phenyl complex") and DCC-type ("Dichloro complex") are nucleophilic in nature, which are incompatible with the electrophilic sulfur cathode [11–14]. In 2011, Muldoon et al. firstly reported that the non-nucleophilic electrolyte ($HMDSMgCl/AlCl_3$ in THF) was suitable for Mg-S battery [15]. Later, although this kind of electrolytes has been further optimized, and it is still limited by the exorbitant price and corrosion problems [16,17]. Inspiringly, the conventional $Mg(TFSI)_2$-based electrolytes have many advantages of good stability, high conductivity, wide electrochemical window, strong solvation ability, and good compatibility with sulfur cathode, showing great application potential. Additionally, because TFSI-based ether solution is still the standard electrolyte for investigating the fundamental properties of

* Corresponding authors.
E-mail addresses: mutiansheng@stu.hit.edu.cn (T. Mu), zuopj@hit.edu.cn (P. Zuo).

https://doi.org/10.1016/j.cej.2022.138663
Received 29 June 2022; Received in revised form 9 August 2022; Accepted 13 August 2022
Available online 17 August 2022

metal-sulfur batteries, it is more conducive to compare the electrochemical behavior of Li-S battery and Mg-S battery [18]. Unfortunately, the $Mg(TFSI)_2$-based electrolytes have long been ruled out due to its incompatibility with Mg metal electrode [19–21]. Until 2018, Wang et al. successfully realized the application of $Mg(TFSI)_2$-based electrolytes for Mg-S battery via Mg-ion conductive interphase formation, and it is also demonstrated that the battery showed high initial capacity (more than 1000 mAh g^{-1}) and high discharge voltage (about the 1.5 V) [22]. Therefore, how to further optimize $Mg(TFSI)_2$-based electrolytes in the follow-up works is particularly meaningful for the high-energy magnesium rechargeable batteries [23–26].

At the same time, the Mg-S battery also suffer from the rapid attenuation of capacity due to the poor reversibility of sulfur electrode [8]. Wang' group attributed this phenomenon to the poor electrochemical activity and low conductivity of the discharge products involving MgS_2/MgS, and accordingly, proposed an effective strategy by introducing lithium salt (LiTFSI) as electrolyte additive to the chemical reactivation intermediate MgS_x [27]. Meanwhile, according to the latest research, Lu et al. revealed that the low solubility of polysulfides in ether solvents is the primary reason for the poor performance [28]. Based on this, the feasibility of high-donor-number solvents such as DMF and DMSO in the sulfur cathode side of Mg-S battery was verified, and the state-of-the-art electrochemical performance of Mg-S battery was obtained [29,30]. However, although the obvious improvement has been achieved by these strategies, it should be mentioned that all these works was based on model batteries, and it is difficult to be extensively applied in coin or pouch batteries. Besides, NuLi et al. also reported that the reversibility of Mg-S battery can be improved by using the Cu current collector in cathode, and at the same time corrosion of Cu collector should be put more attention [31–33]. Therefore, massive efforts are needed to further promote the development of Mg-S batteries [34,35].

In this paper, to enable the $Mg(TFSI)_2$/diglyme electrolytes in RMMBs, an artificial interphase composed of $Zn/ZnCl_2/MgZn_2/MgCl_2$ at Mg electrode interface was pre-produced by substitution reaction between $ZnCl_2$ and Mg at high-temperature condition. As expected, compared with the bare Mg electrode, the interfacial impedance and the Mg plating/stripping overpotential of the modified Mg electrode can be reduced by two orders of magnitude and 10 times, respectively. Combined with the application of the Cu-KB/S cathode using Cu powders as additive in KB/S cathode, the electrochemical performance of Mg-S battery is significantly improved, and the extent of performance improvement is directly proportional to the addition amount of Cu powders. Accordingly, the optimal electrochemical performance can be obtained with a superior capacity of 1160 mAh g^{-1} at 0.1C (based on the sulfur). Even as the current density increases to 0.5C, the battery still shows a capacity of 938 mAh g^{-1} over 120 cycles. In addition, the action mechanism of Cu metal on the electrochemical reaction of sulfur electrode was further explored. The results confirm that the chemical reaction between Cu metal and the intermediate MgS_8 can occur, and the reaction product Cu_2S continues to participate in the electrochemical reaction to eventually form Cu metal and MgS. In the charging process, the discharge product of Cu can be also reacted with MgS by electrochemical oxidation to regenerate Cu_2S. Additionally, the change of redox couple from S/S^{2-} to Cu_2S/Cu^0 will be accomplished during the cycling, which is beneficial to the cycling stability improvement of the magnesium secondary battery.

2. Experimental

2.1. Materials

Tetrahydrofuran (THF) (Analytical Reagent), Dimethyl sulfoxide (DMSO) (Analytical Reagent) and diethylene glycol dimethyl ether (diglyme, DGM, G2) (Analytical Reagent) were purchased from Macklin Co. Ltd and were dehydrated with 4 Å molecular sieves prior to use, then transferred to glove box for storage. Zinc chloride ($ZnCl_2$, 99.95% metals basis) and Magnesium (II) Bis(trifluoromethanesulfonyl)imide ($Mg(TFSI)_2$, >97.0%) were purchased from Aladdin Co. Ltd and were vacuum dried at 120℃ before use to reduce the influence of moisture. The separator (Glass fiber, GF/D) was purchased from Waterman Co. Ltd and cut to discs with a diameter of 16 mm. All three Cu powders samples of different sizes (99.95% metals basis) were purchased from Macklin Co. Ltd without further treatment.

2.2. Fabrication of the artificial interphase and Cu-KB/S cathode

The preparation process of the artificial interphase is as follows: Firstly, the natural oxide layer on the surface of the bare Mg electrode was first removed by sanding, and then polished Mg electrode was cut into round pieces with a diameter of 14 mm. Later, 50 μl solution (0.2 M $ZnCl_2$/THF) was dropped onto the Mg electrode surface and heated to 200 ℃ for 10 min to volatilize the solvent and make replacement reaction.

The specific preparation process of the Cu-KB/S cathode is as follows: Firstly, Ketjenblack carbon/Sulfur (sulfur content of 65 wt%) composite materials were prepared by melt-diffusion method, which can refer to the our previous work[21]. Subsequently, 70 mg active material (KB/S), 20 mg binder (PEO), 10 mg conductive agent (Super-p), and different weights of Cu powder (0/50/100/150/200 mg) were weighed and then grinded together, during which deionized water was added to adjust the viscosity. Next, the evenly slurry was coated on the Al foil (carbon coated) and heated in vacuum at 60 ℃. Finally, the dried electrode was cut into round pieces with a diameter of 14 mm and stored after weighing.

2.3. Mg-S battery preparation and measurements

All electrochemical tests and characterizations were carried out based on coin cell (CR2025), which were assembled as follows: Mg anode (bare or modified), separator (GF/D) and Sulfur cathode (KB/S or Cu-KB/S) were successively placed, during which 80 μl electrolyte (0.5 M $Mg(TFSI)_2$/G2) was adding onto the separator, and then sealed by hydraulic press.

2.4. Characterization and electrochemical tests

The XRD (100-240VAC, 50/60 Hz, 0.6kVA, BRUKER) and the XPS (Resolution:0.48EV, KARTOS) characterizations were conducted to identify the lattice structure and state of element, respectively. Galvanostatic charge/discharge tests of Mg-S batteries were carried out with the Land battery test system of Wuhan Jinnuo Electronics Co., Ltd. Cyclic voltammetry (CV) was measured between 0.01 V and 2.5 V at a rate of 0.1 mV/s with CHI-660A electrochemical workstation. Electrochemical impedance (EIS) measurement was conducted for Mg-Mg systematic cell between 0.1 Hz and 100 kHz with PARSTAT-2273 advanced electrochemical system.

3. Result and discussion

As illustrated in Fig. 1a, the artificial interphase can be obtained by the replacement reaction between $ZnCl_2$ and Mg metal. Firstly, the $ZnCl_2$/THF solution as the reaction reagent is easy to prepare, and its price is relatively lower than that of Bi/Sn/Ge-based solution[24,36,37]. Secondly, since the equilibrium electrode potential of Zn is higher than that of Mg ($E^{2+}_{Zn/Zn} = -0.763$ V vs SHE, $E^{2+}_{Mg/Mg} = -2.3$ V vs SHE), $ZnCl_2$ can easily realize the replacement reaction with Mg metal ($ZnCl_2 + Mg \rightarrow MgCl_2 + Zn$), and the reaction is exothermic ($E_{rxn} = -102$ kJ/mol), which also indicates the spontaneity of the reaction. In order to identify the composition of the artificial interphase, the XRD and XPS tests were carried out for the modified Mg electrode respectively. As determined by the XRD pattern (Fig. 1b), in addition to the diffraction peak of Mg metal

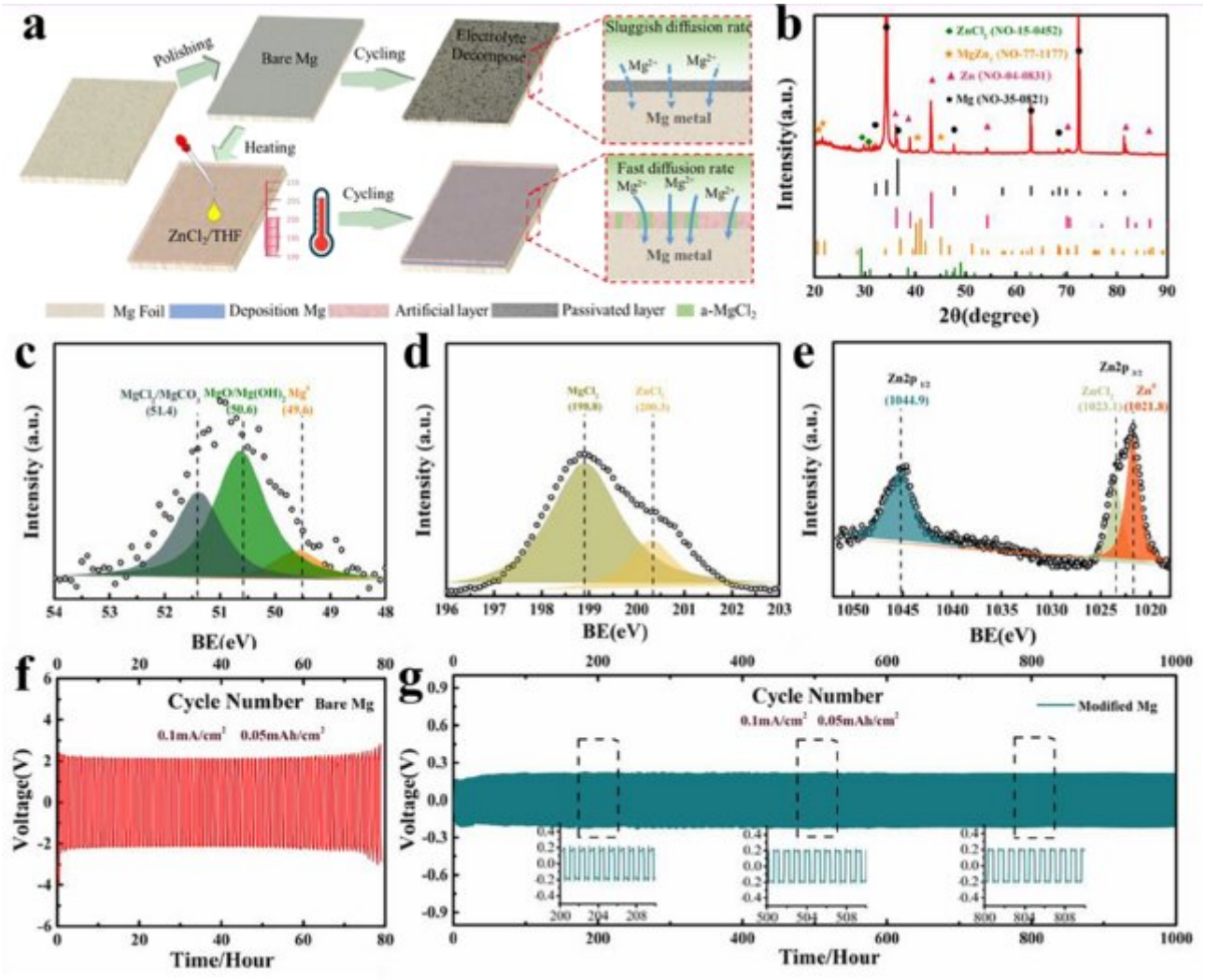

Fig. 1. (a) Schematic illustration of preparation process of artificial interphase; (b) XRD pattern of modified Mg; XPS analysis of the modified Mg surface: (c) Mg 2p, (d) Cl 2p, and (e) Zn 2p; (f-g) Voltage profiles in Mg-Mg symmetric cells using the bare Mg and modified Mg as electrode in 0.5 M $Mg(TFSI)_2$/G2 electrolytes at 0.1 mA/cm^2 for 1/2h discharge and 1/2h charge.

(Mg^0), three obvious characteristic peaks belonging to Zn metal (Zn^0) were detected at 38.8°, 43.2°, and 54.2°, indicating that the replacement reaction occurs ($ZnCl_2 + Mg \rightarrow MgCl_2 + Zn$). At the same time, the characteristic peaks of $MgZn_2$ alloy at 21°, 22.2°, 40.4°, and 45.3° further prove that the alloying reaction will continue between the reaction products of Zn and Mg metal ($Mg + 2Zn \rightarrow MgZn_2$). Furthermore, the diffraction peak intensity of $MgZn_2$ alloy is much lower than that of Zn metal, indicating that only a small amount of the replacement reaction product Zn metal involves in the subsequent alloying reaction, so the content of $MgZn_2$ alloy component is small. Additionally, three weak diffraction peaks at 18.1°, 29.8°, and 69.1° indicate the existence of trace reactants $ZnCl_2$ residue. According to the XPS fitting results on Mg 2p spectrum (Fig. 1c), besides the characteristic peaks of Mg^0 and MgO/$Mg(OH)_2$, the characteristic peak of $MgCl_2/MgCO_3$ at 51.4 eV can be also identified [18,38]. For the Cl 2p spectrum (Fig. 1d), the characteristic peaks at 200.3 and 198.8 eV correspond to $ZnCl_2$ and $MgCl_2$, respectively. Meanwhile, the existence of $Zn^0/ZnCl_2$ was further proved in the Zn 2p spectrum (Fig. 1e). The above analysis results demonstrate that the mechanisms of interfacial reaction are replacement reaction and alloying reaction, and the artificial interphase are composed of Zn/$ZnCl_2/MgZn_2/MgCl_2$. In the case of elemental zinc, it has been proved that the significant lattice mismatch between hexagonal Zn and MgO induces dislocations, leading to a highly defective interphase, which is beneficial to improve the interfacial charge transfer kinetics and reduce the overpotential of Mg electrode[39]. For $MgZn_2$ alloy components, the alloy electrode can induce the generation of a large number of tilt grain boundaries (GBs) at the Mg surface, which can essentially decrease the reaction barriers for both the anodic and cathodic reactions symmetrically and improves the exchange current density[40]. Besides, it has been also proved that Mg-ions in metal halides ($MgCl_2$ and MgI_2) have low ion transport barrier by combining first-principles calculation and ion-transport theory, which can be used as potential Mg electrode coating materials[41]. Therefore, with the help of the above favorable components, even if there is a small amount of passivation components such as $MgCO_3/MgO/Mg(OH)_2$, the artificial interphase still shows excellent Mg-ion transport capability to ensure reversible Mg plating-stripping reaction, accompanied by a small amount of alloying-dealloying reaction. Furthermore, by comparing the interface morphology of the Mg electrodes (Fig.S1a and b), it can be seen that the interface of modified Mg electrode is smoother than bare Mg electrode. Furthermore, the elements of Zn, Mg, Cl and O are evenly distributed on the interface as evidenced in Fig. S1c–g, indicating the good homogeneity of artificial interphase. From the perspective of cross-section (Fig. S2), it can be also observed that the thickness of the artificial interphase is about 6 μm.

To verify the effects of the artificial interphase on Mg plating/

stripping overpotentials, the Mg-Mg symmetric cells using bare or modified Mg as electrodes were assembled and tested for galvanostatic cycles in 0.5 M $Mg(TFSI)_2$/G2 electrolyte. As displayed in Fig. 1f and g, the results reveal that the overpotential of the symmetric cell using modified Mg electrode is about 0.2 V at 0.1 mA/cm^2 (0.05 mAh/cm^2), which is 10 times smaller than that of battery using bare Mg electrode. The symmetric cell can be cycled steadily for 1000 times with a steady overpotential. In Fig. S3, the cycling stability of symmetric cell using modified Mg electrode at higher current density of 0.5 mA/cm^2 was further explored. The symmetric cell can be cycled steadily for 400 times without short-circuit phenomenon. Moreover, the rate performance of symmetric cell was carried out as shown in Fig. S4, and the result demonstrates that the modified Mg electrode with good interfacial properties can ensure reversible plating/stripping reactions with low polarization voltages. The overpotential increases gradually with the applied current densities (0.05, 0.1, 0.2, 0.5 and 1 mA/cm^2). When the current density increases to 1 mA/cm^2, the overpotential reaches 0.3 V, indicating that the low overpotential can be obtained even in relatively high rate for the symmetric modified Mg cells. Meanwhile, the Tafel plots measurements and the electrochemical impedance tests of Mg-Mg symmetrical cells were also carried out in 0.5 M $Mg(TFSI)_2$/G2 electrolyte. With respect to the Tafel plots in Fig. S5a, the apparent exchange-current-density (i_0) responsible for the interface reaction rate at equilibrium can be obtained by fitting Tafel curves in the oxidation process, and it is suggested that the modified Mg electrode possesses higher interfacial reaction kinetics than the bare Mg electrode (lg i_0: -3.35 mA cm^{-2} vs -7.58 mA cm^{-2}). At the same time, the impedance test results (Fig. S5b) show that the interfacial impedance decreases by two orders of magnitude after Mg electrode interface regulation (400 Ω vs 10^5 Ω). In general, these results indicate that the artificial interphase has important effect on the application of $Mg(TFSI)_2$-based electrolytes in RMMBs.

The electrochemical performances of Mg-S batteries based on modified Mg electrode were further investigated in 0.5 M $Mg(TFSI)_2$/G2 electrolyte by constant-capacity charging. As shown in Fig. 2b, the Mg-S battery with KB/S cathode and modify Mg anode shows a discharge voltage plateau of ~1.5 V during the first cycle at the current density of 0.1C (based on sulfur), which is far higher that of the Mg-S battery based on the bare Mg electrode[21]. However, the poor reversibility of sulfur electrode leads to the rapid attenuation of capacity, and the discharge specific capacity is significantly reduced from 1032 mAh/g to 400 mAh/g after 100 cycles (Fig. 2a). Furthermore, the voltage plateau of ~1.5 V also disappears in the subsequent cycles because the initial discharge product (MgS) has poor reoxidation capability to long-chain magnesium polysulfide (MgS_x) in the charging process [8]. In order to further improve the cycling stability of Mg-S battery, the Cu-KB/S cathode was prepared by using Cu powders as additive for KB/S cathode, and the extent of performance improvement is directly proportional to the addition amount of Cu powders. When the amount of Cu powders in composite cathode material is low, the discharge voltage profile of the first cycle shows obvious fluctuation in Fig. 2c. This phenomenon is mainly related to the chemical and electrochemical reaction process of composite cathode materials. In the initial discharge stage, the electrochemical reduction reaction of sulfur (S_8) occurs, and the produced intermediates of long-chain polysulfide magnesium will react chemically with copper metal. Furthermore, the chemical reaction products of short-chain magnesium polysulfide will also react with the residual long-chain magnesium polysulfide or sulfur, affecting the amount of active substances of the cathode. The above reaction process leads to the discharge capacity fluctuation of the battery. With the increase of the mass of Cu powders, the discharge capacity is gradually improved and the discharge voltage platform at 1.0 V is also prolonged (Fig. 2c–f). When the addition amount of Cu powders is 200 mg, the battery shows the optimal electrochemical performances of the initial discharge specific capacity of 1024 mAh/g and the capacity of 1077 mAh/g even after 100 cycles. Moreover, the CV tests for Mg-S batteries with KB/S cathode and Cu-KB/S cathode were carried out respectively, and the battery using Cu-KB/S as cathode has a very obvious reduction peak at ~1.0 V, which is significantly improved in comparison with the reduction peak of ~0.5 V for KB/S cathode (Fig. S6). The Cu powders show positive effect in the electrochemical performance improvement of the rechargeable magnesium batteries. In addition, the effect of Cu metal on the conductivity of cathode was further explored by impedance test. As shown in Fig S7, the electrochemical impedance of Mg-S batteries based

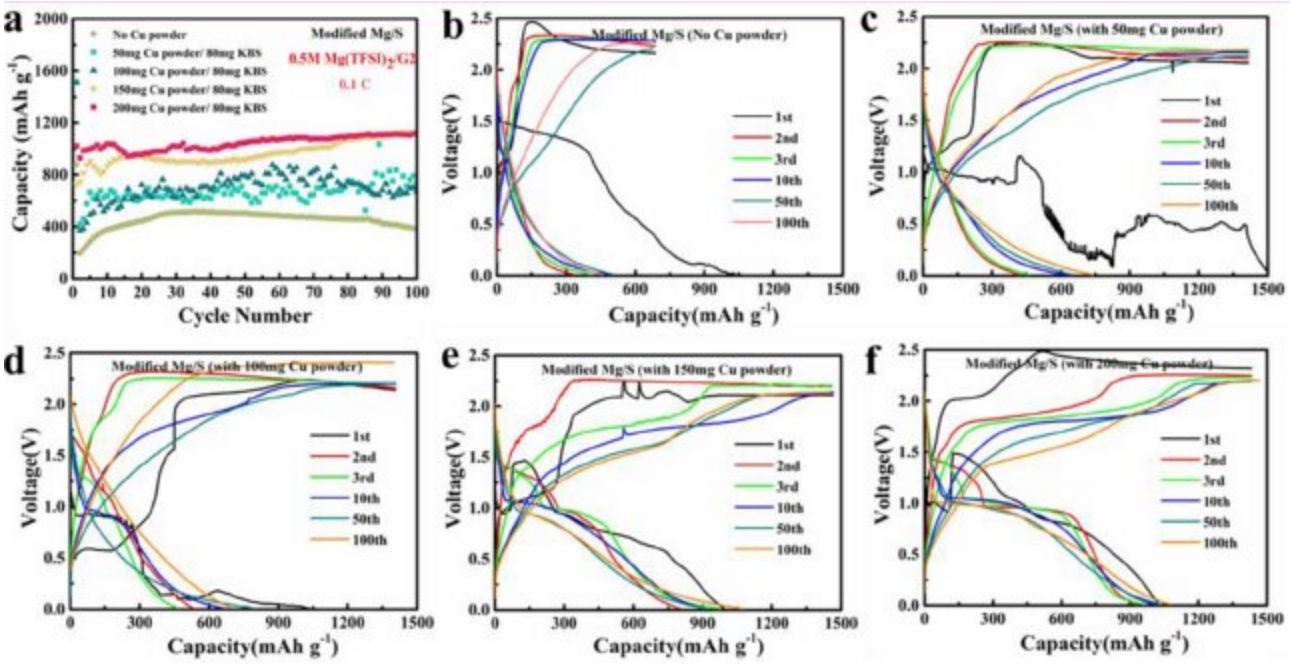

Fig. 2. (a) The cycling performances of Mg-S cells at 0.1C in 0.5 M $Mg(TFSI)_2$/G2 electrolytes with different mass Cu powders as additive and the corresponding voltage profiles of without adding Cu powder (b), adding 50 mg Cu powder (c), adding 100 mg Cu powder (d), adding 150 mg Cu powder (e), and adding 200 mg Cu powder (f).

on KB/S and Cu-KB/S electrodes was tested and fitted according to the equivalent circuit shown in Fig S8. The corresponding parameters of each impedance element are shown in Table S1, it is found that the Cu-KB/S electrode has lower interfacial impedance than the KB/S electrode, indicating that the introduction of copper powder can effectively improve the conductivity of cathode.

Furthermore, the effect of particle sizes of Cu powder on the electrochemical performance of Mg-S batteries was also studied. The SEM images of Cu powders used in the above experiments (Sample 1, Fig. 2) are shown in Fig. 3a and Fig. S9. In addition, the SEM images of the other two Cu powders with larger particle sizes are shown in Fig. 3b and 3c, named sample 2 and sample 3 respectively. It can be clearly observed that sample 1 is composed of some irregular particles with particle size less than 1 μm, and sample 2 with a larger size is formed by aggregation of small particles, and sample 3 with the largest size is a single large particle. Meanwhile, the particle size distribution of the three samples was also characterized by laser particle size analyzer (Fig. 3d), and the mean particle size (D50) are shown in Tab. S2. The results on the particle sizes are in good agreement with the SEM images. In addition, the BET test shows that the specific-surface-area of the three Cu powders decreases gradually with the increasing particle size. Subsequently, three kinds of Cu-KB/S cathode (150 mg Cu/80 mg KB/S) were prepared by using Cu powder with different particle sizes, respectively. The electrochemical performances of Mg-S batteries was tested in 0.5 M Mg $(TFSI)_2$/G2 electrolyte at current density of 0.1C. Unexpectedly, the cycling performance becomes better and better as the particle size of Cu powders increases. As shown in Fig. 3e, when the Cu powder of sample 3 is used as cathode additive, the highest discharge capacity can be achieved, and it can be retained at 1160 mAh/g after 50 cycles. As seen from Fig. 3f and Fig. S11, with the increase of Cu powders particle size, the discharge voltage platform at about 1 V is gradually extended, which shows more capacity for the battery. The XRD tests for the three Cu powders with different particle sizes (Fig. 3g) were conducted, and the results show that the smaller the particle size of Cu powder, the diffraction peak of CuO and Cu_2O is more intense, indicating that smaller Cu powders have higher surface activity and are more likely to react with oxygen or water in the air. Furthermore, a layer of oxide on the surface is not conducive to the pariticipation of the inner Cu metal. Then, the cycling performance at 0.5C and rate performance of Mg-S batteries were tested based on Cu-KB/S cathode using sample 3 as additive. It can be found that the Mg-S battery can deliver an initial discharge capacity of about 800 mAh/g, and the capacity can still be maintained at 938 mAh/g after 120 cycles (Fig. 3h). In addition, when the current density increases from 0.1C to 2C, the discharging capacity gradually decreases. Moreover, it is worth noting that the cyclic stability decreases with the increase of current density, and at the same time the polarization potential increases gradually (Fig. 3i and 3j).

The application of Cu metal can significantly improve the cycling stability of the battery, and it is important to reveal the action mechanism of Cu. First, excess Cu powder was added into the pre-prepared 0.05 M MgS_8/DMSO solution. It can be seen that the brown-red MgS_8/DMSO solution gradually becomes clear and transparent with the

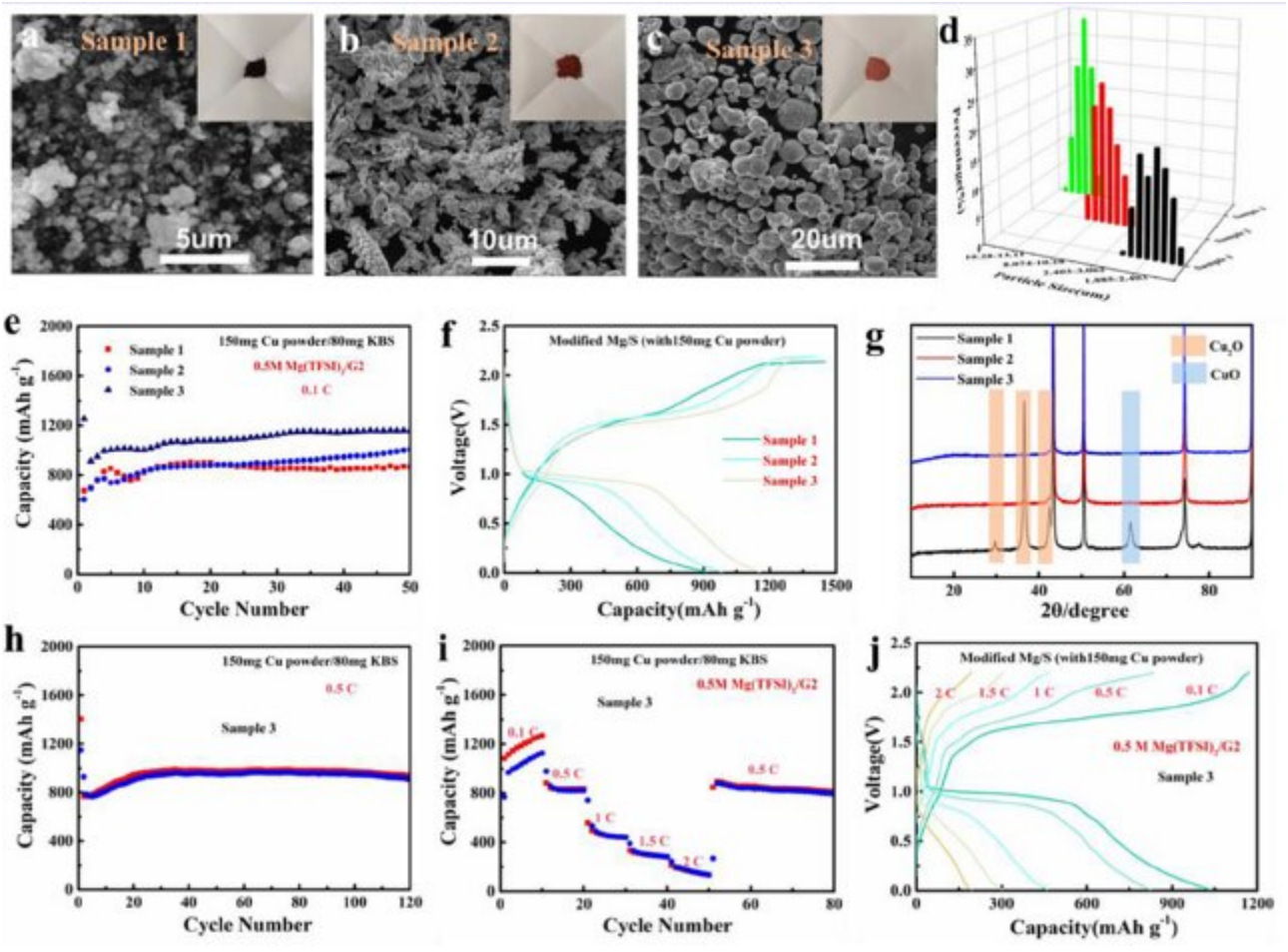

Fig. 3. SEM image of Cu powders of sample 1 (a), sample 2 (b), and sample 3 (c); (d) Particle size distribution of three different Cu powders; (e) The cycling performances of Mg-S full cells using Cu powders of different particle sizes as additives at 0.1C and the corresponding voltage profiles (f); (g) XRD patterns of three different Cu powders; (h) The cycling performances of Mg-S cells using Cu powders of sample 3 as additives at 0.5C; (e) The rate performances of Mg-S cells using Cu powders of sample 3 as additives at 0.1C,0.5C,1.5C, 2C, and 0.5C and (j) the corresponding voltage profiles.

reaction time (Fig. 4a). In the meantime, by comparing the Uv-vis spectra of the solution before and after the reaction, it can be found that the characteristic peaks of S_8^{2-} and S_6^{2-} in the MgS_8/DMSO solution will disappear after reaction in Fig. 4b. These phenomena mentioned above reveal that the chemical reactions can occur between Cu and MgS_8 [31]. In order to identify the specific reaction mechanism, a series of characterization on the Cu powder sediments after the reaction were performed. As evidenced by SEM and EDS in Fig. 4c-g, the rough surface of Cu powder is not only uniformly distributed with a large amount of Cu and S elements, but also with trace Mg elements. Moreover, the XRD test on the Cu powder sediments was also carried out. It is indicated that five obvious characteristic peaks located at 36.2°, 37.4°, 45.9°, 48.3°, and 53.8° can be assigned to Cu_2S, and two weak characteristic peaks located at 34.4° and 49.3° can be attributed to MgS (Fig. 4i). Moreover, the XPS test results of the Cu powder sediments also further confirm the existence of the reaction products Cu_2S and MgS. Therefore, the chemical reaction between Cu and MgS_8 can be inferred as: $MgS_8 + 14Cu \rightarrow 7Cu_2S + MgS$.

Based on the understanding on the chemical reaction mechanism between Cu and MgS_8, the influence mechanism of Cu metal on the electrochemical conversion reaction of sulfur electrode was further explored by XRD tests on Cu-KB/S electrode at different charge and discharge stages (Fig. 5a). It can be noticed that the diffraction peak intensities of MgS at 34.4° and 49.3° increase gradually with the discharge process, but decrease gradually at the subsequent charging stage. However, the variation tendency of characteristic peak intensities of Cu_2S at 37.4°, 45.9°, and 48.3° is opposite to that of MgS. The peak intensities will first decrease with discharging and then increase with charging. It should be mentioned that the characteristic peak of Cu metal (Cu^0) occurs at 43° during the discharge process, and the corresponding peak intensity increases gradually. In the charging stage, the characteristic peak intensity of Cu^0 gradually weakens and finally disappears, which is opposite to that of discharge stage. At the same time, the XPS measurements also were conducted for the Cu-KB/S cathode at different charging and discharging stages, and the fitted test results are shown in Fig. 5b and c. It can be seen that during the discharge process, the fitting peak intensity of MgS at 161.6 eV increases gradually, while the peak intensity of Cu_2S at 162.1 eV and solid phase MgS_x (such as MgS_2) at 162.1 eV decreases gradually. During the charging process, the changes of the peak intensity are opposite to that of the discharge stage. Moreover, the variation law of fitting peak intensities of MgS and Cu_2S are consistent with the XRD results.

According to the above results, the specific reaction mechanism of the Cu-KB/S cathode can be deduced. During the discharge process, the electrochemical reduction reaction of solid phase S_8 first occurs, and soluble S_8^{2-} anions is generated in ether-based electrolytes (Eq. (1)).

$$S_8 + 2e^- \rightarrow S_8^{2-}$$

Subsequently, the S_8^{2-} anions dissolved in the electrolytes diffuse near the Cu metal inside the cathode, and then chemical reaction will occur with each other (Eq. (2)), resulting in the formation of Cu_2S and MgS in the solid phase.

$$S_8^{2-} + 14Cu + Mg^{2+} \rightarrow 7Cu_2S + MgS$$

At the same time, the part of S_8^{2-} anions will still undergo electrochemical reduction reactions, from soluble long-chain polysulfide to insoluble short-chain polysulfide (Eqs. (3) to (5)).

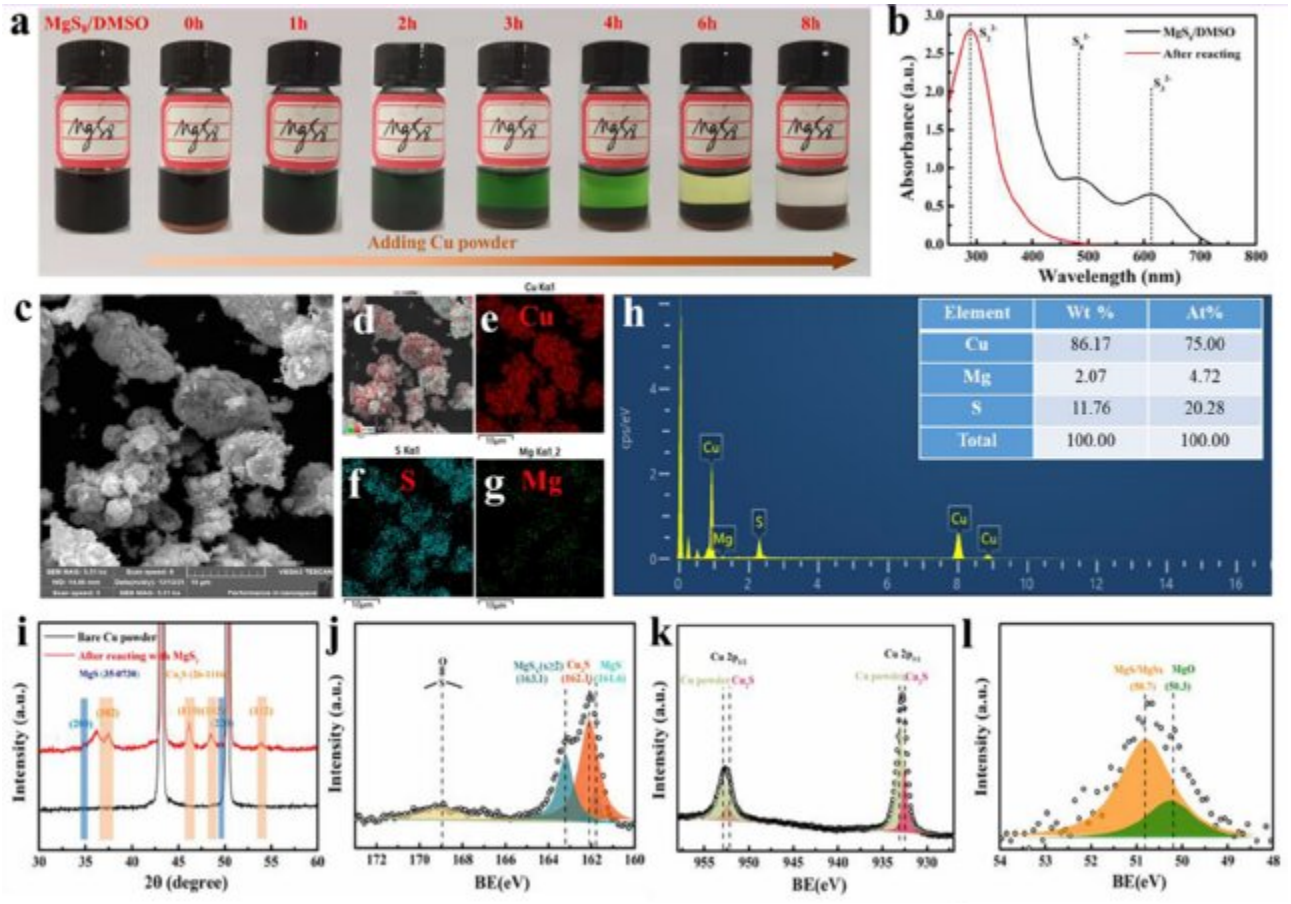

Fig. 4. (a) Optical photos of Cu powder and MgS_8/DMSO solution at different reaction periods; (b) UV-spectra of the supernatant before and after the reaction; (c) SEM image of Cu powders after reaction and the corresponding elemental mapping images of total (d), Cu (e), S (f), and Mg (g); (h) Element content on the Cu powders surface after reaction; (i) XRD patterns of the Cu powders after reaction;XPS spectra of the Cu powders after reaction: (j) S 2p, (k) Cu 2p, (l) Mg 2p.

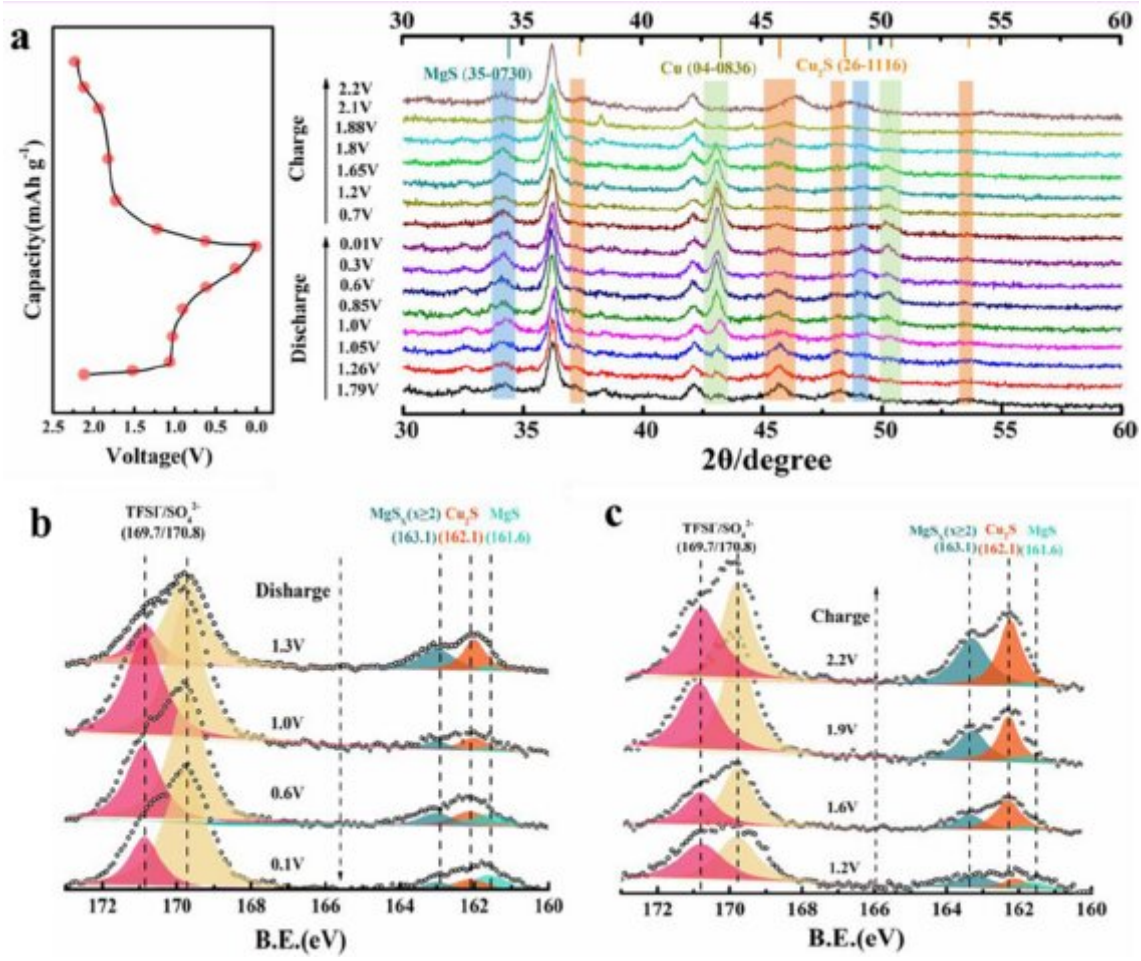

Fig. 5. (a) The XRD patterns and (b-c) the XPS spectra of Cu-KB/S cathode at different steps of dis- and charge process.

$S_8^{2-} + 2e^- \rightarrow 2S_4^{2-}$

$S_4^{2-} + 2e^- \rightarrow 2S_2^{2-}$

$S_2^{2-} + 2e^- \rightarrow 2S^{2-}$

On the side, the further electrochemical reaction between Cu_2S generated in reaction (2) and Mg ions occur to form Cu metal and MgS (Eq. (6)).

$Cu_2S + 2e^- + Mg^{2+} \rightarrow 2Cu + MgS$

In the charging process, as the discharge product of MgS has poor electrochemical activity, it is difficult to re-oxidize to the long-chain MgS_x or S_8 (Eq. (7)). The discharge product of Cu metal has high electronic conductivity, and it can promote the electrochemical conversion of MgS to regenerate Cu_2S ((Eq. (8))[42].

$8S^{2-} - 16e^- \rightarrow S_8$

$2Cu + MgS - 2e^- \rightarrow Cu_2S + Mg^{2+}$

Additionally, as the cycle number increases, the proportion of the redox reaction of sulfur decreases gradually. Ultimately, the change of redox couple from S/S^{2-} to Cu_2S/Cu^0 will be accomplished during the cycling, and the soluble intermediate magnesium polysulfide will also not produce during the charging and discharging process, which is beneficial to improve the cycling stability of secondary magnesium battery. Besides, according to the above reaction mechanism, when the ratio of Cu/S atoms is 2:1, the conversion of all sulfur to Cu_2S is realized and the best electrochemical performance can be obtained. It follows that 80 mg KB/S (sulfur content of 65 wt%) requires 206 mg Cu metal to achieve complete conversion. Therefore, the electrochemical performance of Cu-KB/S electrode is gradually optimized with the increase of the addition amount of Cu metal, and the best performance is achieved when the addition amount of Cu metal reaches 200 mg.

4. Conclusion

In this work, an artificial interface composed of $Zn/ZnCl_2/MgZn_2/MgCl_2$ was prepared by ion exchange reaction between $ZnCl_2$ and Mg metal. At the current density of 0.1 mA cm^{-2} (0.05 mAh cm^{-2}), the modified Mg electrode not only can deliver low Mg plating/stripping overpotential (~0.2 V) in $Mg(TFSI)_2$/DGM electrolyte, but also shows superior cycling stability. On this basis, the effect of Cu powders as cathode additive on the electrochemical performance of Mg-S batteries was further systematically explored. The electrochemical test results reveal that the Cu-KB/S cathode exhibits higher cycling stability than the KB/S cathode. Furthermore, by means of a series of test characterization (Uv-Vis, SEM and ex-situ XRD and XPS), it can be inferred that the introduction of Cu powder fundamentally changes the reaction mechanism of sulfur cathode mainly due to the chemical reaction between the Cu metal and the intermediate magnesium polysulfide (MgS_8), which can eventually transform the redox couples of S/S^{2-} into the Cu/Cu_2S. In addition, the influence of the particle size and addition amount of Cu powder on the performance of KB/S cathode was investigated, and it is pointed out that balancing the mount and particle size of Cu powders is important to the performance improvement of the KB/S

cathode. These studies not only elucidate the reaction mechanism of Cu metal on the electrochemical reaction of sulfur electrode, but also provide reference for the development of rechargeable magnesium batteries in the future.

Declaration of Competing Interest

The authors declare that they have no known competing financial interests or personal relationships that could have appeared to influence the work reported in this paper.

Data availability

Data will be made available on request.

Acknowledgments

The authors acknowledge and thank for financially supporting from the National Natural Science Foundation of China (no. 51772068), the Key-Area Research and Development Program of Guangdong Province (no. 2020B090919005), the Key Research and Development Program of Heilongjiang Province (no. GA21A102) and the Fundamental Research Funds for the Central Universities (Grant No. HIT.OCEF.2021008).

Appendix A. Supplementary data

Supplementary data to this article can be found online at https://doi.org/10.1016/j.cej.2022.138663.

References

[1] Z. Liang, C. Ban, Strategies to Enable Reversible Magnesium Electrochemistry: From Electrolytes to Artificial Solid-Electrolyte Interphases, Angew Chem Int Ed Engl 60 (20) (2021) 11036–11047.
[2] D.-T. Nguyen, R. Horia, A.Y.S. Eng, S.-W. Song, Z.W. Seh, Material design strategies to improve the performance of rechargeable magnesium-sulfur batteries, Materials Horizons 8 (3) (2021) 830–853.
[3] F. Xiong, Y. Jiang, L.i. Cheng, R. Yu, S. Tan, C. Tang, C. Zuo, Q. An, Y. Zhao, J.-J. Gaumet, L. Mai, Low-strain TiP_2O_7 with three-dimensional ion channels as long-life and high-rate anode material for Mg-ion batteries, Interdisciplinary Materials 1 (1) (2022) 140–147.
[4] J. Wang, S. Tan, G. Zhang, Y. Jiang, Y. Yin, F. Xiong, Q. Li, D. Huang, Q. Zhang, L. Gu, Q. An, L. Mai, Fast and stable Mg2+ intercalation in a high voltage NaV2O2(PO4)2F/rGO cathode material for magnesium-ion batteries高电压镁离子电池正极材料NaV2O2(PO4)2F/rGO快速和稳定的Mg2+嵌入, Science China Materials 63 (9) (2020) 1651–1662.
[5] W. Yan, J.L. Yang, X. Xiong, L. Fu, Y. Chen, Z. Wang, Y. Zhu, J.W. Zhao, T. Wang, Y. Wu, Versatile Asymmetric Separator with Dendrite-Free Alloy Anode Enables High-Performance Li-S Batteries, Adv Sci (Weinh) (2022) e2202204.
[6] J. Ruan, H. Sun, Y. Song, Y. Pang, J. Yang, D. Sun, S. Zheng, Constructing 1D/2D interwoven carbonous matrix to enable high-efficiency sulfur immobilization in Li-S battery, Energy Materials (2021).
[7] J. Castillo, L. Qiao, A. Santiago, X. Judez, A.S. de Buruaga, G. Jimenez, M. Armand, H. Zhang, C. Li, Perspective of polymer-based solid-state Li-S batteries, Energy Materials (2022).
[8] T. Gao, X. Ji, S. Hou, X. Fan, X. Li, C. Yang, F. Han, F. Wang, J. Jiang, K. Xu, C. Wang, Thermodynamics and Kinetics of Sulfur Cathode during Discharge in MgTFSI2 -DME Electrolyte, Adv Mater 30 (3) (2018) 1704313.
[9] A. Robba, A. Vizintin, J. Bitenc, G. Mali, I. Arčon, M. Kavčič, M. Žitnik, K. Bučar, G. Aquilanti, C. Martineau-Corcos, A. Randon-Vitanova, R. Dominko, Mechanistic Study of Magnesium-Sulfur Batteries, Chemistry of Materials 29 (2017) 9555–9564.
[10] Y. Lu, C. Wang, Q. Liu, X. Li, X. Zhao, Z. Guo, Progress and Perspective on Rechargeable Magnesium-Sulfur Batteries, Small Methods 5 (5) (2021) 2001303.
[11] R.J.H. Thomas, D. Gregory, R.C. Winterton, Nonaqueous Electrochemistry of Magnesium, J. Electrochem. Soc 137 (1990) 775–780.
[12] D. Aurbach, Z. Lu, A. Schechter, Y. Gofer, H. Gizbar, R. Turgeman, Y. Cohen, M. Moshkovich, E. Levi, Prototype systems for rechargeable magnesium batteries, Nature 407 (2000) 724–727.
[13] O. Mizrahi, N. Amir, E. Pollak, O. Chusid, V. Marks, H. Gottlieb, L. Larush, E. Zinigrad, D. Aurbach, Electrolyte Solutions with a Wide Electrochemical Window for Rechargeable Magnesium Batteries, Journal of The Electrochemical Society 155 (2) (2008) A103.
[14] N. Pour, Y. Gofer, D.T. Major, D. Aurbach, Structural analysis of electrolyte solutions for rechargeable Mg batteries by stereoscopic means and DFT calculations, J Am Chem Soc 133 (2011) 6270–6278.
[15] H.S. Kim, T.S. Arthur, G.D. Allred, J. Zajicek, J.G. Newman, A.E. Rodnyansky, A. G. Oliver, W.C. Boggess, J. Muldoon, Structure and compatibility of a magnesium electrolyte with a sulphur cathode, Nat Commun 2 (2011) 427.
[16] Z. Zhao-Karger, X. Zhao, D.i. Wang, T. Diemant, R.J. Behm, M. Fichtner, Performance Improvement of Magnesium Sulfur Batteries with Modified Non-Nucleophilic Electrolytes, Advanced Energy Materials 5 (3) (2015) 1401155.
[17] C. Liao, N. Sa, B. Key, A.K. Burrell, L. Cheng, L.A. Curtiss, J.T. Vaughey, J.-J. Woo, L. Hu, B. Pan, Z. Zhang, The unexpected discovery of the $Mg(HMDS)_2/MgCl_2$ complex as a magnesium electrolyte for rechargeable magnesium batteries, Journal of Materials Chemistry A 3 (11) (2015) 6082–6087.
[18] T. Gao, S. Hou, K. Huynh, F. Wang, N. Eidson, X. Fan, F. Han, C. Luo, M. Mao, X. Li, C. Wang, Existence of Solid Electrolyte Interphase in Mg Batteries: Mg/S Chemistry as an Example, ACS Appl Mater Interfaces 10 (17) (2018) 14767–14776.
[19] N.N. Rajput, X. Qu, N. Sa, A.K. Burrell, K.A. Persson, The coupling between stability and ion pair formation in magnesium electrolytes from first-principles quantum mechanics and classical molecular dynamics, J Am Chem Soc 137 (9) (2015) 3411–3420.
[20] Y. Li, P. Zuo, R. Li, M. He, Y. Ma, Y. Shi, X. Cheng, C. Du, G. Yin, Electrochemically-driven interphase conditioning of magnesium electrode for magnesium sulfur batteries, Journal of Energy, Chemistry 37 (2019) 215–219.
[21] R. Zhang, C. Cui, R. Li, Y. Li, C. Du, Y. Gao, H. Huo, Y. Ma, P. Zuo, G. Yin, An artificial interphase enables the use of $Mg(TFSI)_2$-based electrolytes in magnesium metal batteries, Chemical Engineering Journal 426 (2021) 130751.
[22] X. Li, T. Gao, F. Han, Z. Ma, X. Fan, S. Hou, N. Eidson, W. Li, C. Wang, Reducing Mg Anode Overpotential via Ion Conductive Surface Layer Formation by Iodine Additive, Advanced Energy Materials 8 (7) (2018) 1701728.
[23] Y. Zhang, J. Li, W. Zhao, H. Dou, X. Zhao, Y. Liu, B. Zhang, X. Yang, Defect-Free Metal-Organic Framework Membrane for Precise Ion/Solvent Separation toward Highly Stable Magnesium Metal Anode, Adv Mater 34 (6) (2022) 2108114.
[24] J. Luo, Y. Xia, J. Zhang, X. Guan, R. Lv, Enabling Mg metal anodes rechargeable in conventional electrolytes by fast ionic transport interphase, National Science Review 7 (2020) 333–341.
[25] H. Park, H.-K. Lim, S.H. Oh, J. Park, H.-D. Lim, K. Kang, Tailoring Ion-Conducting Interphases on Magnesium Metals for High-Efficiency Rechargeable Magnesium Metal Batteries, ACS Energy Letters 5 (12) (2020) 3733–3740.
[26] Y. Sun, Q. Zou, W. Wang, Y.-C. Lu, Non-passivating Anion Adsorption Enables Reversible Magnesium Redox in Simple Non-nucleophilic Electrolytes, ACS Energy Letters 6 (10) (2021) 3607–3613.
[27] T. Gao, M. Noked, A.J. Pearse, E. Gillette, X. Fan, Y. Zhu, C. Luo, L. Suo, M. A. Schroeder, K. Xu, S.B. Lee, G.W. Rubloff, C. Wang, Enhancing the reversibility of Mg/S battery chemistry through Li(+) mediation, J Am Chem Soc 137 (38) (2015) 12388–12393.
[28] Q. Zou, Y. Sun, Z. Liang, W. Wang, Y.-C. Lu, Achieving Efficient Magnesium-Sulfur Battery Chemistry via Polysulfide Mediation, Advanced Energy Materials 11 (31) (2021) 2101552.
[29] G. Bieker, J. Wellmann, M. Kolek, K. Jalkanen, M. Winter, P. Bieker, Influence of cations in lithium and magnesium polysulphide solutions: dependence of the solvent chemistry, Phys Chem Chem Phys 19 (18) (2017) 11152–11162.
[30] G. Bieker, D. Diddens, M. Kolek, O. Borodin, M. Winter, P. Bieker, K. Jalkanen, Cation-Dependent Electrochemistry of Polysulfides in Lithium and Magnesium Electrolyte Solutions, The Journal of Physical Chemistry C 122 (38) (2018) 21770–21783.
[31] A. Du, Y. Zhao, Z. Zhang, S. Dong, Z. Cui, K. Tang, C. Lu, P. Han, X. Zhou, G. Cui, Selenium sulfide cathode with copper foam interlayer for promising magnesium electrochemistry, Energy Storage Materials 26 (2020) 23–31.
[32] A. Robba, M. Mežnar, A. Vizintin, J. Bitenc, J. Bobnar, I. Arčon, A. Randon-Vitanova, R. Dominko, Role of Cu current collector on electrochemical mechanism of Mg-S battery, Journal of Power Sources 450 (2020), 227672.
[33] L. Zeng, N. Wang, J. Yang, JiuLin Wang, Y. NuLi, Application of a Sulfur Cathode in Nucleophilic Electrolytes for Magnesium/Sulfur Batteries, Journal of The Electrochemical Society 164 (12) (2017) A2504. A2512.
[34] Y. Xu, Y. Ye, S. Zhao, J. Feng, J. Li, H. Chen, A. Yang, F. Shi, L. Jia, Y. Wu, X. Yu, P.-A. Glans-Suzuki, Y.i. Cui, J. Guo, Y. Zhang, In Situ X-ray Absorption Spectroscopic Investigation of the Capacity Degradation Mechanism in Mg/S Batteries, Nano Lett 19 (5) (2019) 2928–2934.
[35] H. Fan, Z. Zheng, L. Zhao, W. Li, J. Wang, M. Dai, Y. Zhao, J. Xiao, G. Wang, X. Ding, H. Xiao, J. Li, Y. Wu, Y. Zhang, Extending Cycle Life of Mg/S Battery by Activation of Mg Anode/Electrolyte Interface through an LiCl-Assisted $MgCl_2$ Solubilization Mechanism, Advanced Functional Materials 30 (2019) 1909370.
[36] Y. Zhao, A. Du, S. Dong, F. Jiang, Z. Guo, X. Ge, X. Qu, X. Zhou, G. Cui, A Bismuth-Based Protective Layer for Magnesium Metal Anode in Noncorrosive Electrolytes, ACS Energy Letters 6 (7) (2021) 2594–2601.
[37] J. Zhang, X. Guan, R. Lv, D. Wang, P. Liu, J. Luo, Rechargeable Mg metal batteries enabled by a protection layer formed in vivo, Energy Storage Materials 26 (2020) 408–413.
[38] H.D. Yoo, S.-D. Han, I.L. Bolotin, G.M. Nolis, R.D. Bayliss, A.K. Burrell, J. T. Vaughey, J. Cabana, Degradation Mechanisms of Magnesium Metal Anodes in Electrolytes Based on $(CF_3SO_2)_2N(-)$ at High Current Densities, Langmuir 33 (37) (2017) 9398–9406.
[39] H.P. Jiwoong Bae, X. Guo, X. Zhang, J.H. Warner, Y.u. Guihua, High-performance magnesium metal battery via switching passivation film into solid electrolyte interphase, Energy & Environmental Science 14 (2021) 4391–4399.
[40] H.-K. Tian, R. Jalem, M. Matsui, T. Mandai, H. Somekawa, Y. Tateyama, Tuning the performance of a Mg negative electrode through grain boundaries and alloying

toward the realization of Mg batteries, Journal of Materials Chemistry A 9 (27) (2021) 15207–15216.
[41] T. Chen, G. Sai Gautam, P. Canepa, Ionic Transport in Potential Coating Materials for Mg Batteries, Chemistry of Materials 31 (2019) 8087–8099.
[42] B. Lee, J. Choi, S. Na, D.-J. Yoo, J.H. Kim, B.W. Cho, Y.-T. Kim, T. Yim, J.W. Choi, S.H. Oh, Critical role of elemental copper for enhancing conversion kinetics of sulphur cathodes in rechargeable magnesium batteries, Applied Surface Science 484 (2019) 933–940.